Directional wave separation in tubular acoustic systems - the development and evaluation of two industrially applicable techniques

DOI:
10.1016/j.apacoust.2016.09.003

Document Version
Accepted author manuscript

Directional wave separation in tubular acoustic systems - the development and evaluation of two industrially applicable techniques

K.H. Groves[a,*], B. Lennox[a]

[a] *School of Electrical and Electronic Engineering, The University of Manchester, Room E1, Sackville Street Building, Granby Row, Manchester, United Kingdom, M1 3BU*

Abstract

An acoustic device is used to evaluate internal features and defects within tubes by determination of the acoustic impulse response. This paper concerns methods of separating the total pressure wave measured in the device into its forward and backward travelling components, which facilitates computation of the acoustic impulse response. The device comprises a tube that has a speaker at one end and is axially instrumented with microphones. Unlike similar works, the methods presented in this paper were designed to be applied in an industrial context, they allow simple calibration and implementation using readily transportable equipment. Two wave separation algorithms are presented; the first is a known method that has been improved to provide simplified calibration and the second is a computationally inexpensive technique that has been adapted to improve its operational bandwidth. The techniques are critically evaluated using a custom built test rig, designed to simulate realistic tube features and defects such as constrictions, holes and corrosion. It is demonstrated that, although inter-microphone attenuation is not accounted for in the second algorithm, both algorithms function well and give similar results. It is concluded that the added sophistication of the first method means that it is less affected by low frequency interference and is capable of yielding more accurate results. However, in practical use as an evaluation tool, the benefits of including inter-microphone attenuation are outweighed by the additional calibration and computational requirements. Finally the output of the wave separation techniques is validated by showing agreement between experimental impulse response measurements and those obtained from a theoretically derived acoustic tube simulator.

Keywords: Acoustic pulse reflectometry; non destructive evaluation; pipe inspection; system identification; speaker; multiple microphones.

*Corresponding author. Tel.: +44161 306 2045

Email addresses: keir.groves@manchester.ac.uk (K.H. Groves), barry.lennox@manchester.ac.uk (B. Lennox)

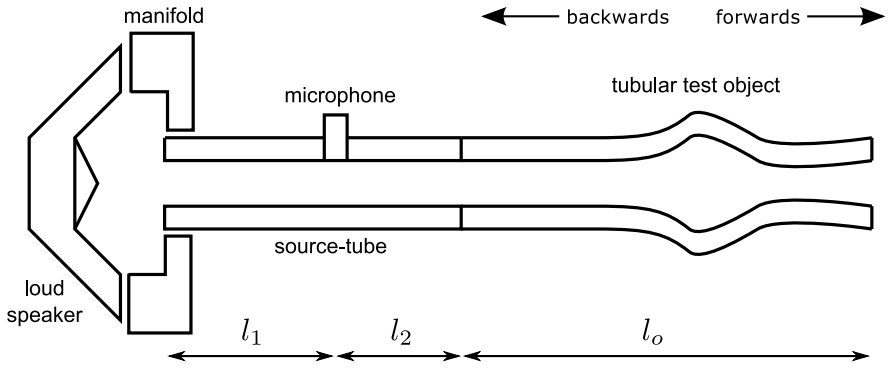

Figure 1: Typical APR testing arrangement

1. Introduction

Acoustic pulse reflectometry (APR) is a proven method of characterising features and profiles within tubular objects. APR has various applications, including measurement of the bore profile of musical instruments [1–3], determination of features of the vocal tract [4, 5] and, as is the focus here, non destructive evaluation (NDE) of industrial tubes and pipelines [6–8]. Not only is APR an effective method for the detection, location and characterisation of features and defects within tubes and pipelines, it is non-invasive as nothing is physically inserted in the tube. Testing on single tubes can be performed in a matter of seconds, and APR is deployable on live pipelines as it is tolerant to static pressure, flow and a wide variety of gas compositions. On this basis APR is highly suited to industrial use; however, much of the relevant literature [2, 4, 9–12] is focused on laboratory based experiments where little attention is focused on the industrial applicability of the methods. The present paper offers two methods of APR testing that can be readily deployed in an industrial context.

A common shortcoming of APR systems is that the impulse response of an object can be difficult to interpret due to the presence of re-reflected waveforms. With reference to Figure 1, sound is injected into the gas (air) within the source-tube by the speaker, travels forwards into the test object and is reflected back towards the speaker wherever it encounters a change in acoustic impedance; returning pressure waves are then re-reflected at the manifold/speaker location and again travel forwards through the source-tube and into the test object. If there is an overlap of forward and backward propagating waves at the microphone location then the response of the test object cannot be isolated from the response of

the system to the left of the microphone, i.e. the speaker and manifold. This problem can be overcome by separating the total pressure wave into its forward and backward travelling components. If wave separation is implemented and the forward and backward travelling waves are isolated at a given axial location within the source-tube, backward travelling waves (the output) may be deconvolved with respect to forward travelling waves (the input) to achieve the impulse response of the system to the right of the given location, i.e. the acoustic impulse response of the test object.

Wave separation may be achieved by using a long source-tube [11]. Setting l_2 greater than half the length of the excitation waveform; $l_2 > c/2\lambda$, (where c is the speed of sound in the tube and λ is the length of the waveform) and l_1 greater than l_O, (Figure 1) ensures firstly, that the outgoing wave fully passes the microphone before the reflection from the test object is received; and secondly, that reflections from any feature in the test object pass the microphone before the recorded signal is corrupted by forward travelling re-reflections. However, the use of long source-tubes is unfavorable because of the added acoustic attenuation, limitations on the length of the excitation signal and general impracticality of transporting and connecting a long tube. An alternative is to decompose overlapping pressure waves into their forward and backward travelling components using two or more axially spaced microphones within the source-tube [2, 4, 13, 14]. While using just two microphones is advantageous for its simplicity and minimal interruption within the source-tube, the fundamental drawback of any two microphone wave separation technique is that a singularity occurs when an acoustic wavelength within the tube is equal to twice the inter-microphone distance, or integer multiples thereof [14]. It is critical to note that one of the singularities is at zero frequency. The frequency band (from zero upwards) over which the first singularity is dominant reduces with increasing microphone spacing. Therefore a trade off is made between overall bandwidth and loss of signal to noise at low frequencies. Combining the results of more than one microphone pairs can significantly alleviate this trade-off [2, 14, 15].

For a wave separation technique to be deployed as part of an NDE tool in an industrial context three key issues must be considered.

1. Frequency content; for APR to be beneficial in the NDE sector it must be possible for long tubes (5 m and above) to be tested, as such low frequency content must be measured and included in subsequent processing. There are two key reasons for this; first, low frequencies are less affected by attenuation and so can travel greater distances without significant loss of signal; second, long test objects have resonances at lower frequencies than short objects and if an undistorted time domain impulse response is to be achieved all resonances must be captured by the system. Within the relevant literature, test object lengths are rarely greater than 1 m [2, 4, 9–12] and as such frequencies below ≈ 100 Hz are commonly neglected since they contain no resonances. Kemp et al. [2] fitted a straight line to the frequency response below 100 Hz, this was valid since the longest object tested was less than 250 mm in length. If for example a 5 m object is to

be tested, resonances could be expected at frequencies as low as 17 Hz, based on a quarter wavelength resonance and assuming a speed of sound of 342 m/s; so the interpolated straight line could only be applied in the sub 10 Hz range. This means that for wave separation to be implemented in longer tubes, frequency range of the measurements must be extended as close to zero as possible.

2. The system output should be a time domain impulse response of the object under test. The acoustic response of tubular objects is often determined in terms of an object's planar mode complex input impedance [16]. Although the acoustic impedance is closely related to the impulse response [14], the impulse response is most appropriate as this gives the clearest indication of defect location and associated feature shape.
3. Calibration must be simple, fast and not reliant on the use of numerous or long calibration load tubes. For example, in [12] a high accuracy acoustic impedance measurement technique is presented that uses three calibration loads, one of which is a 97 m pipe. Such a calibration would be inappropriate in an industrial context due to the requirement to have on hand a 97 m tube and sensitivity of the method of [12] to the quality of connection with the source-tube.

In the present work two methods of multi-microphone wave separation are developed to make them suitable for use in an industrial NDE tool. A rigorous high accuracy technique that requires some on-site calibration is compared to a faster, less rigorous method that requires no on-site calibration. The two wave separation techniques used are both known methods; however, in their raw form neither method is suitable for deployment in an industrial APR system. As such, modifications are made to both techniques to improve their accuracy and usability. The first technique, introduced by Kemp et al. [2], is a time domain multi-microphone technique that includes the effects of inter-microphone attenuation. Modifications made to this technique simplify the on-site calibration procedure and remove restrictions on microphone spacing while maintaining its salient benefits. The second technique, developed by Louis et al. [4], is analogous to the first although inter-microphone attenuation is not included. In fact, the methods may be shown to be equivalent for a two microphone system where Kemp's multi-microphone transfer functions are replaced by pure delays. The benefits of the method of Louis et al. [4] is that its mathematical formulation allows for fast processing and, by not including inter-microphone attenuation, calibration requirements are minimal. The technique given by Louis et al. [4] is modified in the present work so that it is applicable to multi-microphone systems, therefore expanding the frequency band over which it may be applied.

Both separation techniques assume plane wave propagation and constant operating conditions. The plane wave assumption holds true until the upper limit frequency (around 10.86 kHz for an 18.6 mm tube in room temperature air) is approached [14]. Constant propagation conditions are assumed, although they only need be assumed over the length of a single test as calibration adjustments

can be performed between tests if the operating conditions of a tube bundle are changing rapidly.

2. Experimental setup

A schematic of the experimental setup used throughout this work is shown in Figure 2. The source-tube is constructed of extruded aluminium tube with an internal diameter of 18.6 mm and outer diameter of 25.4 mm. Three axially spaced Sennheiser KE4-211 omni-directional capsule microphones were installed in the source-tube wall at the same radial location. To ensure that the microphones cause as small an interruption in the source-tube as possible an optimal fitting technique was developed. A blind hole with the same diameter as the microphone is machined into the outer wall of the source-tube, the hole depth is set to leave only a small amount of material between the bottom of the hole and the internal wall of the source-tube. A 2 mm centre drill is then passed through this thin section of material. The microphone is installed in the hole, pressed up against the shoulder and hermetically sealed in place with adhesive sealant. Data output and acquisition was implemented using a National Instruments USB-4431 signal acquisition module coupled with a PC running LabVIEW®, sampling was performed simultaneously across all channels at 96 kHz using a suitable in line anti-aliasing filter. Acoustic excitation was provided by a Fostex FX-120 full range driver, selected for its low reaching and relatively flat frequency response; an Alpine PMX-T320 amplifier was connected between the the National Instruments module and the driver. The Fostex driver was connected to the source-tube by a custom designed manifold; the manifold was designed and constructed such that the combined frequency response of the speaker and manifold system was as flat as could be achieved over the functional bandwidth of the system.

3. Modification of the wave separation technique of Kemp et al.

3.1. Overview of the waveguide technique

The waveguide technique of Kemp et al. is presented in [2] and the Matlab® script used in the present work is available in the supporting material, therefore only a basic overview of how the algorithm is implemented for a two microphone setup is detailed in the present section. Once a two microphone algorithm is defined, expanding to three or more microphones is a relatively simple process.

Before the wave separation algorithm can be implemented it is necessary to determine the $n_m\,(n_m - 1)$ inter-microphone transfer functions, where n_m is the number of microphones. For the case of two microphones there are two transfer functions: the transfer function of a forward travelling wave from microphone one to microphone two $\boldsymbol{h_{12}}$ and the transfer function of a backwards travelling

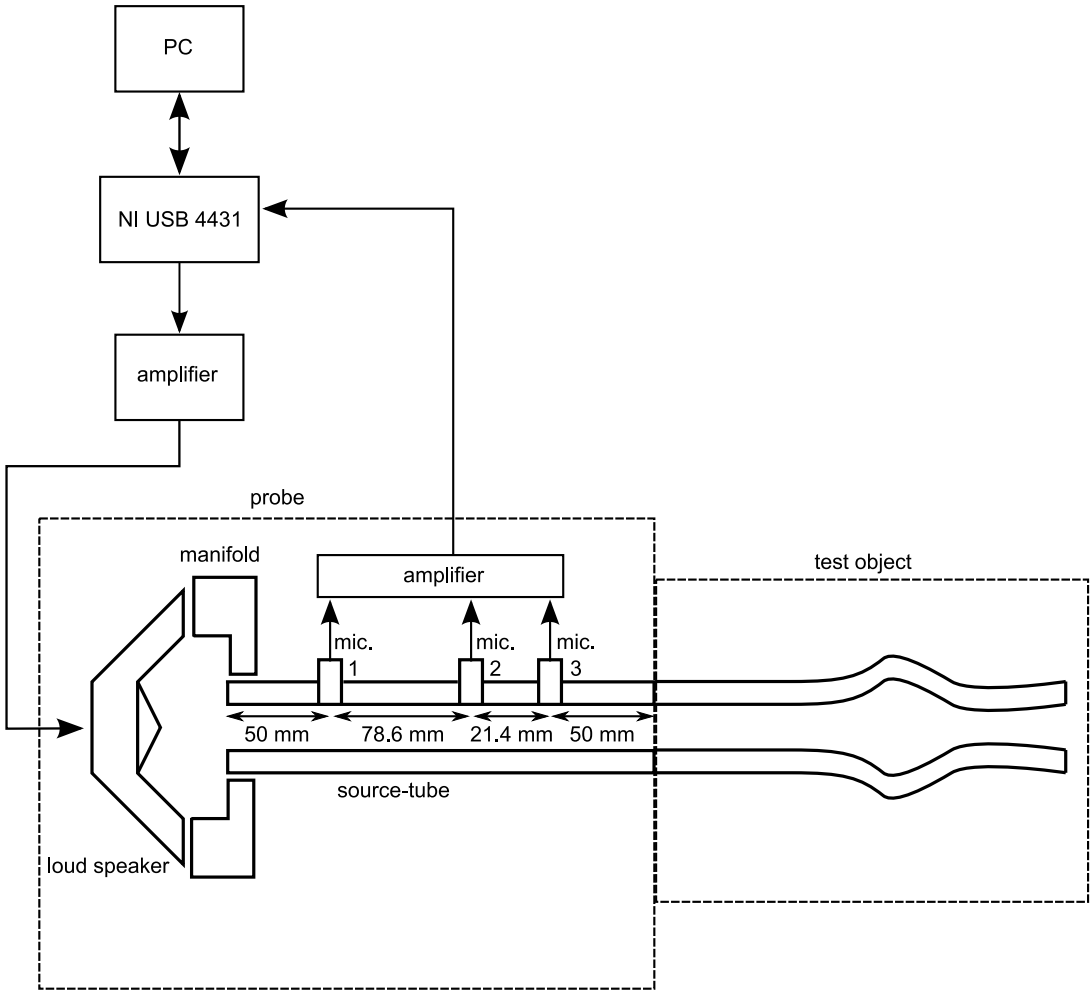

Figure 2: Experimental setup used throughout the work

wave from microphone two to microphone one $\boldsymbol{h_{21}}$. The transfer functions $\boldsymbol{h_{12}}$ and $\boldsymbol{h_{21}}$ are realised in discrete time as finite length impulse response signals. Following the determination of the inter-microphone functions, which is discussed in Section 3.2, it is possible to implement the wave separation algorithm.

It is the purpose of the wave separation technique to separate the recorded microphone signals into their forward and backward travelling components. Sound is injected into the source-tube and the resulting pressure signal at each microphone is recorded and stored as two vectors, $\boldsymbol{p_1}$ and $\boldsymbol{p_2}$. Since the tubular acoustic system is assumed to be linear and time invariant (LTI), the microphone signals $\boldsymbol{p_1}$ and $\boldsymbol{p_2}$ may be equated to the sum of their forward and backward travelling components, $\boldsymbol{p_1} = \boldsymbol{p_1^+} + \boldsymbol{p_1^-}$ and $\boldsymbol{p_2} = \boldsymbol{p_2^+} + \boldsymbol{p_2^-}$. Wave separation using a waveguide is a causal method based on step by step time domain convolution of directional pressure signals with the appropriate inter-microphone transfer functions. The waveguide method relies on the assumption that there are no acoustic waves travelling in the source-tube for a period of time prior to sound being injected by the speaker. To start the process, four directionally decomposed vectors $\boldsymbol{p_1^+}$, $\boldsymbol{p_1^-}$, $\boldsymbol{p_2^+}$ and $\boldsymbol{p_2^-}$ of length $n_h + n_p$ are initialised, where n_h is the number of points used in the inter-microphone transfer functions and n_p is the number of points in the microphone signals $\boldsymbol{p_1}$ and $\boldsymbol{p_2}$. The first n_h values of the directionally decomposed vectors are set to zero; this is the pre-padding required to begin the separation process. The remaining n_p points of the four vectors of directional waves may now be computed using the following recursive algorithm, for $i = n_h$ to $i = n_h + n_p - 1$:

$$p_2^+(i+1) = \sum_{j=1}^{n_h} p_1^+(i - n_h + j)\, h_{12}(j) \tag{1}$$

$$p_1^-(i+1) = \sum_{j=1}^{n_h} p_2^-(i - n_h + j)\, h_{21}(j) \tag{2}$$

$$p_2^-(i+1) = p_2(i - n_h + 1) - p_2^+(i+1) \tag{3}$$

$$p_1^+(i+1) = p_1(i - n_h + 1) - p_1^-(i+1) \tag{4}$$

Equation 1 uses the current value of the forward travelling wave at microphone one, together with its time history, to predict the forward travelling wave at microphone two at the next time step by convolution with the transfer function $\boldsymbol{h_{12}}$. Similarly, in Equation 2 the backwards travelling wave at microphone two, with its time history, is convolved with $\boldsymbol{h_{21}}$ to calculate the backward travelling wave at microphone one at the next time step. Since the total pressure at each microphone for every time step ($\boldsymbol{p_1}$ and $\boldsymbol{p_2}$) is known, it is possible to calculate the missing components of the directionally decomposed waves (Equations 3 and 4) using the components calculated in Equations 1 and 2. Once the two components of the pressure signal at both microphones have been computed for the next time step, the time step must be incremented and the process repeated until $\boldsymbol{p_1^+}$, $\boldsymbol{p_1^-}$, $\boldsymbol{p_2^+}$ and $\boldsymbol{p_2^-}$ are evaluated in full.

3.2. Determination of inter-microphone transfer functions

The method employed by Kemp et al. [2] to obtain the inter-microphone transfer functions $\boldsymbol{h_{ab}}$ is deconvolution of the recording at one microphone $\boldsymbol{p_b}$ with respect to the recording at another $\boldsymbol{p_a}$ by frequency domain division. Frequency domain deconvolution of $\boldsymbol{p_b}$with respect to $\boldsymbol{p_a}$ is performed as follows:

$$\check{\boldsymbol{h_{ab}}} = \mathcal{F}^{-1}\left(\frac{\mathcal{F}\left(\boldsymbol{p_b}\right)}{\mathcal{F}\left(\boldsymbol{p_a}\right)}\right) \tag{5}$$

where $\mathcal{F}$ is used to denote the discrete Fourier transform and $\mathcal{F}^{-1}$ its inverse. The output of Equation 5 is low pass filtered, with pass and stop bands designed to suit the bandwidth of the denominator. This is necessary because at frequencies where $\mathcal{F}\left(\boldsymbol{p_a}\right) \approx 0$, division by a very small number causes spikes in the frequency response of $\boldsymbol{h_{ab}}$. Kemp et al. [2] provide the mathematical proof that the time domain transfer function between microphones $\boldsymbol{h_{ab}}$ may be separated from $\check{\boldsymbol{h_{ab}}}$ by time domain windowing provided that $\check{\boldsymbol{h_{ab}}}$ begins at zero and returns to zero before the first reflection. However, although beginning and returning to near zero is entirely possible, beginning and returning to zero itself is an impossible condition to meet. This is due to the fact that $\check{\boldsymbol{h_{ab}}}$ is identified over for the full length of $\boldsymbol{p_b}/\boldsymbol{p_a}$; meaning that even if $\check{\boldsymbol{h_{ab}}}$ could be obtained without reflections, $\boldsymbol{h_{ab}}$ would still be non-zero at the end of the window. The low pass filter applied to $\check{\boldsymbol{h_{ab}}}$ spreads the impulsive transfer function which exacerbates the issue at the end of the window and generally causes the first element of $\boldsymbol{h_{ab}}$ to become nonzero also. If the first element of $\boldsymbol{h_{ab}}$ is nonzero then the filter is strictly no longer valid in a causal system since it contains reference to future values. Kemp et al. [17] address the issue of non-zero first elements by allowing the filters to be non-causal and performing wave separation in the frequency domain, however, the issue at the end of the window is not addressed in [2] or [17].

To overcome the shortcomings of the above method, a time domain technique using adaptive least mean square (LMS) filtering is proposed in this paper to obtain the inter-microphone functions. A source-tube run out (a plane length of tube cut from the same stock as the source-tube and attached in place of the test object) was fitted to increase the length of signal that may be considered to contain no backwards travelling waves. Repeated short burst white noise signals were used to excite the acoustic system; the signal used was rebuilt each time the excitation was produced using a random number generator. The signals recorded at each microphone ($\boldsymbol{p_1}$, $\boldsymbol{p_2}$ and $\boldsymbol{p_3}$) were windowed in the time domain to ensure that they contained no reflected backwards travelling waves (giving $\boldsymbol{p_1^+}$, $\boldsymbol{p_2^+}$ and $\boldsymbol{p_3^+}$). The inter-microphone filters $\boldsymbol{h_{12}}$, $\boldsymbol{h_{13}}$ and $\boldsymbol{h_{23}}$ were initialised with zeros and using the windowed microphone signals $\boldsymbol{p_1^+}$, $\boldsymbol{p_2^+}$ and $\boldsymbol{p_3^+}$ as input and output data, the filters were updated using the LMS adaptive algorithm. The step size μ of the adaptive filtering algorithm was kept deliberately low so that the filter did not fully optimise with respect to

each segment of training data, rather, for each short burst of randomly generated training data the filter coefficients $\boldsymbol{h_{ab}}$ update by a small amount. This is a fundamental facet of effective learning: it means that each burst of excitation data need not contain all of the information necessary to identify the system, hence the changing excitation signal. It also ensures that the learning process is tolerant of noise and measurement error since no single measurement has a dominant effect on the final filter. All adaptive filtering was implemented using LabVIEW®'s adaptive filter toolkit. For a filter of order n, the point by point LMS scheme uses the error signal,

$$e\left(i\right) = p_b\left(i\right) - \boldsymbol{h_{ab}}\left(i\right) \cdot \boldsymbol{p_a}(i) \tag{6}$$

to update filter coefficients $\boldsymbol{h_{ab}}$ in the usual way:

$$\boldsymbol{h_{ab}}\left(i+1\right) = \boldsymbol{h_{ab}}\left(i\right) + \mu\, e\left(i\right)\, \boldsymbol{p_a}\left(i\right) \tag{7}$$

where $\boldsymbol{h_{ab}}\left(i\right)$ is the inter-microphone filter coefficients at point i, μ is the step size, $p_b\left(i\right)$ is the desired output and $\boldsymbol{p_a}\left(i\right) = \left[p_a\left(i\right), p_a\left(i-1\right), \ldots, p_a\left(i-n+1\right)\right]$ is the appropriate section of the input vector.

3.3. Inference of backwards inter-microphone transfer functions

To determine both the forward and backward travelling inter-microphone functions, Kemp et al. [2] make two calibration measurements; one with the source-tube in its normal orientation and one with the source-tube flipped so that the speaker effectively directs sound backwards down the source-tube. This arrangement is impractical in an industrial context since it is time consuming and requires disassembly and reassembly of the equipment. As an alternative, a calibration method that does not require any change in the equipment or additional measurements has been developed.

Using the same data collected in 3.2, to obtain the backward travelling transfer functions $\boldsymbol{h_{21}}$, $\boldsymbol{h_{31}}$ and $\boldsymbol{h_{32}}$ the recorded microphone signals $\boldsymbol{p_1^+}$, $\boldsymbol{p_2^+}$ and $\boldsymbol{p_3^+}$ are reversed, such that the first element becomes the last and vice versa, giving $\boldsymbol{p_{1\leftarrow}^+}$, $\boldsymbol{p_{2\leftarrow}^+}$ and $\boldsymbol{p_{3\leftarrow}^+}$. The reversed waves are then used, as if they were backward traveling, to update the coefficients of the transfer functions $\boldsymbol{\hat{h}_{21}}$, $\boldsymbol{\hat{h}_{31}}$ and $\boldsymbol{\hat{h}_{32}}$ using the adaptive filtering technique described in Section 3.2.

Now, $\boldsymbol{\hat{h}_{21}}$, $\boldsymbol{\hat{h}_{31}}$ and $\boldsymbol{\hat{h}_{32}}$ are not equivalent to $\boldsymbol{h_{21}}$, $\boldsymbol{h_{31}}$ and $\boldsymbol{h_{32}}$ because reversing the signals has the effect of inverting attenuation, so it would appear that sound waves increase in amplitude as they travel along the tube. To rectify this, the inferred backwards travelling inter-microphone transfer functions $\boldsymbol{\hat{h}_{21}}$, $\boldsymbol{\hat{h}_{31}}$ and $\boldsymbol{\hat{h}_{32}}$ must be filtered to account for the inverted attenuation. Using the method of Amir et al [18] of converting Keefe's frequency domain filter [19] into the time domain, it is possible to construct the appropriate discrete filter. The attenuation filter must be built such that it emulates attenuation within the source-tube over a length of twice the relevant inter-microphone spacing; one

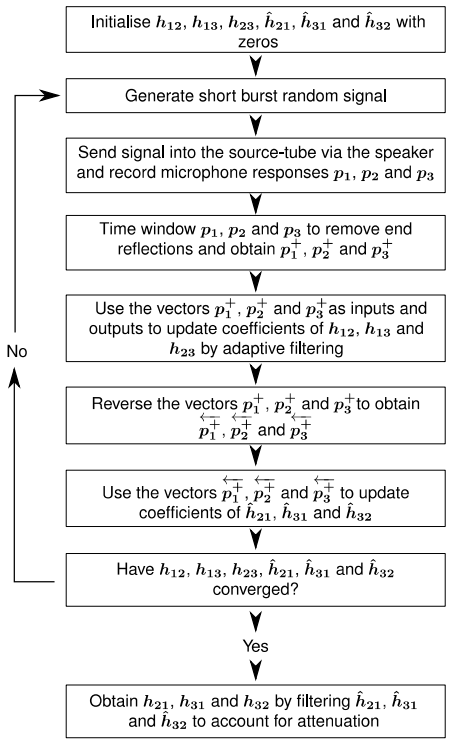

Figure 3: Flow diagram showing the method used to obtain the six directional inter-microphone transfer functions $\boldsymbol{h_{12}}$, $\boldsymbol{h_{13}}$, $\boldsymbol{h_{23}}$, $\boldsymbol{h_{21}}$, $\boldsymbol{h_{31}}$ and $\boldsymbol{h_{32}}$ by adaptive filtering

length will remove the amplification effect and the second length adds the attenuation present between the microphones. Convolution of the inferred backwards travelling filters $\hat{\boldsymbol{h}}_{\boldsymbol{21}}$, $\hat{\boldsymbol{h}}_{\boldsymbol{31}}$ and $\hat{\boldsymbol{h}}_{\boldsymbol{32}}$ with the appropriate attenuation filters results in the correct backward travelling inter-microphone transfer functions $\boldsymbol{h_{21}}$, $\boldsymbol{h_{31}}$ and $\boldsymbol{h_{32}}$. Using the reversed forward signals to obtain backwards traveling transfer functions is valid since it is assumed the microphones and source-tube are not directionally sensitive, therefore $\hat{\boldsymbol{h}}_{\boldsymbol{21}}$, $\hat{\boldsymbol{h}}_{\boldsymbol{31}}$ and $\hat{\boldsymbol{h}}_{\boldsymbol{32}}$ contain the individual microphone response characteristics. Figure 3 shows a flow diagram of the steps used to obtain the six inter-microphone filters $\boldsymbol{h_{12}}$, $\boldsymbol{h_{13}}$, $\boldsymbol{h_{23}}$, $\boldsymbol{h_{21}}$, $\boldsymbol{h_{31}}$ and $\boldsymbol{h_{32}}$.

4. Wave separation by frequency domain signal merging

The method described here is a wave separation technique that maintains the salient properties of the method above, but benefits from algorithmic simplicity and trades off the inclusion of inter-microphone attenuation for negating the necessity for on site calibration. The technique is an expansion of the approach

of Louis et al. [4] that reduces bandwidth limitations. The fundamental concept is to combine impulse responses gained from multiple sets of two microphone systems. The procedure is described here for a three microphone system but may be directly expanded to include any number of additional microphones.

The key steps of the process are as follows. The system is excited by a broadband signal and the responses of the three microphones are recorded. The recorded signals are multiplied by a gain factor to account for sensitivity differences between the microphones, giving $\boldsymbol{p_1}$, $\boldsymbol{p_2}$ and $\boldsymbol{p_3}$. The separation technique of Louis et al. [4] (detailed in AppendixA and available with this article as supporting material) is then used to decompose $\boldsymbol{p_1}$, $\boldsymbol{p_2}$ and $\boldsymbol{p_3}$ into forward and backward travelling components about microphone three. It should be noted that the separation technique of Louis et al. [4] does not provide the forward and backward travelling waves directly, rather we achieve the sum of time shifted versions of the forward and backward waves about a given location, chosen as microphone three in this case. From $p_1(t)$ and $p_3(t)$ it is possible to obtain $p_3^+(t+\tau_{31}) - p_3^+(t-\tau_{31})$ and $p_3^-(t+\tau_{31}) - p_3^-(t-\tau_{31})$, where τ_{13} is the time delay between microphones one and three. Since the system is assumed to be LTI, deconvolution of $p_3^-(t+\tau_{31}) - p_3^-(t-\tau_{31})$ with respect to $p_3^+(t+\tau_{31}) - p_3^+(t-\tau_{31})$ results in the impulse response of the system to the right of microphone three obtained using microphones one and three $\boldsymbol{h_{sys31}}$. Similarly, $p_2(t)$ and $p_3(t)$ are used to obtain $p_3^+(t+\tau_{32}) - p_3^+(t-\tau_{32})$ and $p_3^-(t+\tau_{32}) - p_3^-(t-\tau_{32})$ and deconvolution gives the impulse response of the system to the right of microphone three obtained using microphones two and three $\boldsymbol{h_{sys32}}$. Deconvolution is performed using frequency domain division as per Equation 5.

As discussed in Section 1, both $\boldsymbol{h_{sys31}}$ and $\boldsymbol{h_{sys32}}$ contain singularities at frequencies that are integer multiples of $c/2l$, where c is the speed of sound in the tube and l is the inter-microphone spacing. In Figure 4 examples of magnitude responses of $\boldsymbol{H_{sys31}}$ and $\boldsymbol{H_{sys32}}$ are plotted, where $\boldsymbol{H_{sys31}}$ and $\boldsymbol{H_{sys32}}$ are frequency domain representations of $\boldsymbol{h_{sys31}}$ and $\boldsymbol{h_{sys32}}$. The singularity in $\boldsymbol{H_{sys31}}$ at integer multiples of $\approx 1600\,\mathrm{Hz}$ is clearly visible as well as the singularity in $\boldsymbol{H_{sys32}}$ at $\approx 8000\,\mathrm{Hz}$. In $\boldsymbol{H_{sys31}}$ the singularity occurs at a lower frequency than in $\boldsymbol{H_{sys32}}$, however, at low frequencies $\boldsymbol{H_{sys32}}$ is more affected by the singularity at zero frequency and $\boldsymbol{H_{sys31}}$ yields preferable results. It is possible to exploit the benefits of both pairs of responses by combining $\boldsymbol{H_{sys31}}$ and $\boldsymbol{H_{sys32}}$ in the frequency domain (giving $\boldsymbol{H_{sys321}}$) and taking the inverse Fourier transform of the resulting signal to obtain $\boldsymbol{h_{sys321}}$. $\boldsymbol{H_{sys31}}$ and $\boldsymbol{H_{sys32}}$ are combined by taking the low frequency content of $\boldsymbol{H_{sys31}}$ and fading into $\boldsymbol{H_{sys32}}$ before the singularity in $\boldsymbol{H_{sys31}}$ degrades the signal. Simple linear fading was deemed appropriate since $\boldsymbol{H_{sys31}}$ and $\boldsymbol{H_{sys32}}$ are the same function measured by different microphone pairs. Following the inverse Fourier transform, $\boldsymbol{h_{sys321}}$ is low pass filtered to remove the effect of the singularity in $\boldsymbol{h_{sys32}}$.

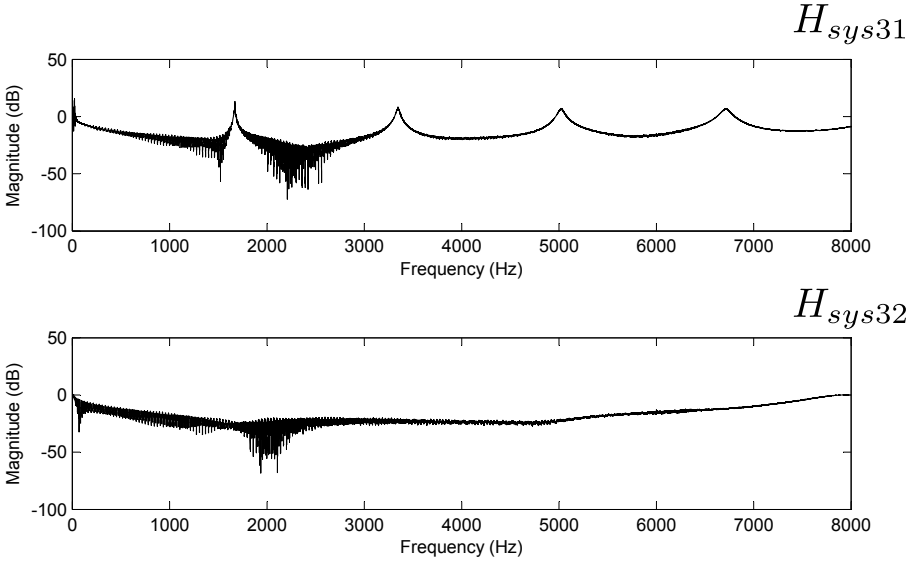

Figure 4: Example plots of $\boldsymbol{H_{sys31}}$ and $\boldsymbol{H_{sys32}}$ against frequency - data plotted is from the testing of tube 1 in Section 5

5. Experiments and validation

5.1. Experimental setup

To compare the relative merits of the wave separation algorithms detailed in Sections 3 and 4 a test rig comprising two 11 m tubes, each containing three features was fabricated. The tubes were constructed of extruded aluminum, had a nominal internal diameter of 18.8 mm and nominal outer diameter of 25.4 mm. The features were designed to replicate a range of defects commonly found in used industrial tubing, e.g. corrosion pitting, blockages and failed joints. To demonstrate the effects of attenuation, the erosion feature is present at different locations in both of the tubes. While designing and fabricating the tubes, due care was taken to ensure that where the tubes had been joined minimal internal interruption resulted and the tube remained airtight. Figure 5 gives details of the features that were machined into the two tubes. It should be noted that the pit defect and the through hole are not radial defects and as such may cause local breakdown of the plane wave assumption.

Prior to testing, six 200 point inter-microphone impulse response functions, necessary to implement the waveguide algorithm, were determined as per Section 3. The device, as depicted in Figure 2, was connected to the tubes in the test rig in turn. Each tube was excited by a logarithmic sine sweep of length 2^{21} samples, the sweep ran from 15 Hz to 8 kHz and was played four times back to back. The average of the second to fourth sequences was used as the input for the wave

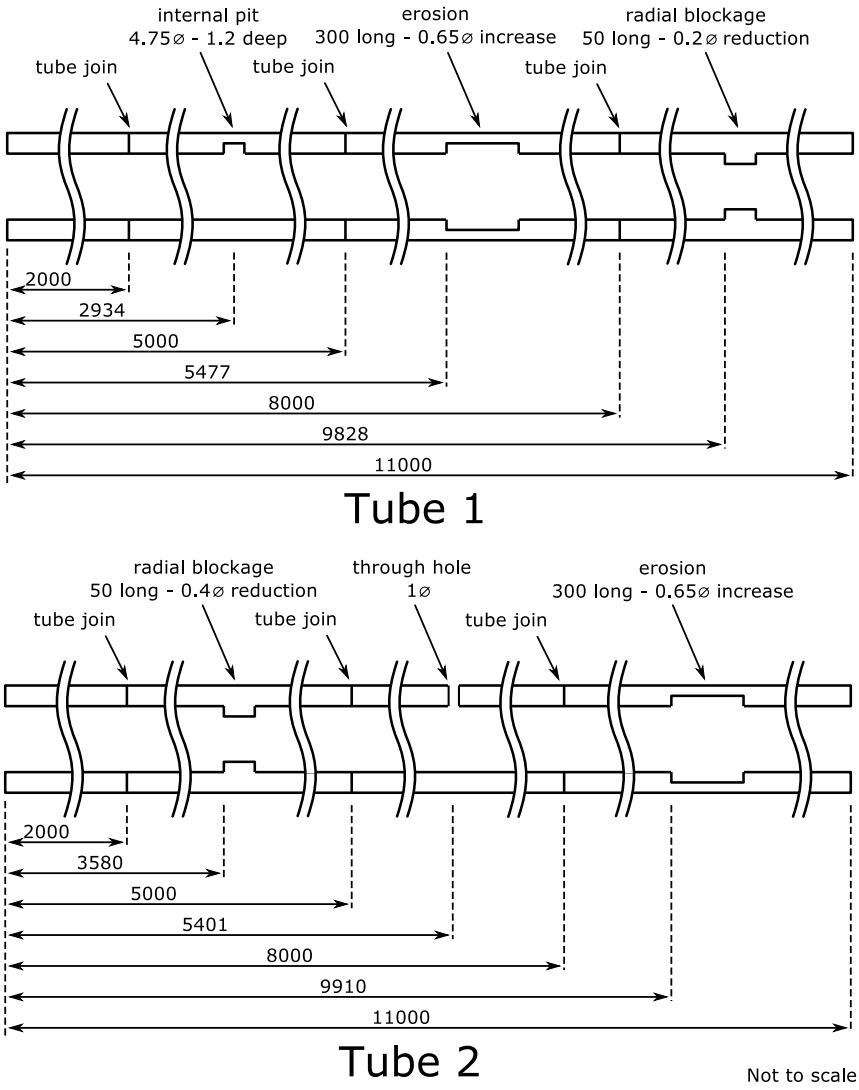

Figure 5: Details of the features present in the two tubes used in experiments - all measurements are in millimeters (mm)

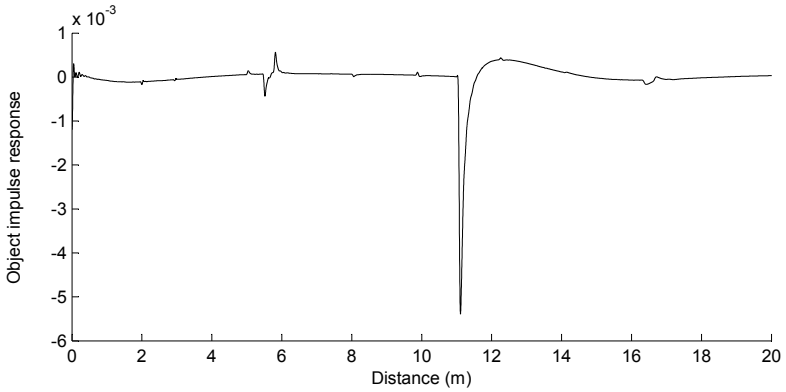

Figure 6: Wide view of the impulse response of tube 1 computed using the waveguide algorithm

separation algorithms. Using a signal whose length was an integer power of two and was pre-padded with itself provided an effective method of predisposing the recorded signal to frequency domain using the fast Fourier transform (FFT) algorithm. Pre-padding ensured that both input and output were periodic while using an integer power of two samples meant that the FFT algorithm could be used. The averaged cyclic data was processed using both of the aforementioned wave separation algorithms. The 2^{21} point forward and backward travelling waves were deconvolved about microphone three using frequency domain division as per Equation 5. Resulting impulse response signals were filtered using a 100 order low pass FIR Chebyshev window filter, designed such that frequency components above 6 kHz were reduced by 100 dB.

Figure 6 shows the impulse response of tube 1 computed using the waveguide technique (Section 3); the purpose of this plot is to offer a wide view of the impulse response of a the tube, giving context to subsequent plots (Figures 7 and 8) where scaling is optimised for displaying smaller features so that the results may be analysed in detail. For ease of interpretation, the x-axis has been converted from time of flight, t, to distance, d, according to $d = {}^{tc}/_{2}$. The speed of sound, c, was calculated from the measured ambient temperature of 21.8 °C according to [19]. In Figure 6 the end of the tube at 11 m is clearly evident, showing its characteristic inverted spike shape. The effects of attenuation may also be observed in the end of tube signature: The signal drops almost vertically at 11 m and the following rise is slower and a tail has developed. At $\approx$16.5 m an internal re-reflection of the erosion defect is seen. This is caused by sound waves leaving the device, reflecting backwards at the open end, reflecting forwards on the erosion defect and finally reflecting backwards again on the open end before travelling back to the source-tube.

5.2. Comparative testing

In Figure 7 the impulse response of tube 1, computed using the waveguide technique, is plotted alongside the impulse response attained using the frequency domain merging method. It is clear that by using either technique the smallest features in the tube can be identified. The small pit at 2.934 m is visible, correctly located and exhibits the expected shape, a drop followed by a rise, caused by the increase followed by reduction in the tube cross section. At 5.477 m the 300 mm long erosion is also clearly visible, the signal from both the increase in cross section at the start of the erosion and the drop in cross section at the end of the erosion are uniquely present and shaped as would be expected. The radial blockage at 9.828 m appears clearly in the response and gives the expected signal shape, a rise followed by a fall. Impulse responses for tube 2 (Figure 8) confirm the efficacy of both techniques at locating and characterising features. The 1 mm ⌀ through hole at 5.401 m is evident and matches a classical hole signature, a drop followed by slow rise and slight overshoot [20]. It is observed that in both tubes reflections are caused by the tube joints at 2 m, 5 m and 8 m; discussion of these features is provided in the final paragraph of Section 5.3.

Although both techniques produce satisfactory results, there are some differences in the plots and neither algorithm gives a perfect reading. It is apparent in Figures 7 and 8 that in the region directly following connection to the device (0-1 m) the results obtained via the waveguide algorithm exhibit a higher level of noise, suggesting that the waveguide algorithm may be more susceptible to poor coupling between the device and test object. In all four plots in Figures 7 and 8 some low frequency interference is present. The interference is less notable in the responses generated using the waveguide algorithm but is present in both. Investigation by the authors has shown that low frequency interference is primarily due to the singularity present in the wave separation algorithms at zero frequency. This is evidenced by the fact that when the impulse response of the system as a whole about one microphone is derived from the same recorded data, by deconvolving the recording at microphone three (for example) with respect to the input excitation signal, low frequency interference is removed. Further evidence is that using larger drivers with lower frequency response and pressure transducers capable of measuring down to zero frequency gave only a small reductions in the low frequency interference. It is important to note that the low frequency interference was repeatable and therefore cannot be entirely put down to SNR issues near to the singularity. This repeatability is likely caused by a lack of accuracy of the inter-microphone transfer functions at low frequency. This fits with the results since the waveguide method provides better representation of the inter-microphone transfer functions, but their performance at low frequency will be diminished due to their relatively short length (200 points), hence the presence of some interference.

Aside from the low frequency interference, it is apparent that both techniques give extremely similar results. The size and shape of signal features in both plots are almost identical. From a practical perspective, the benefits of the

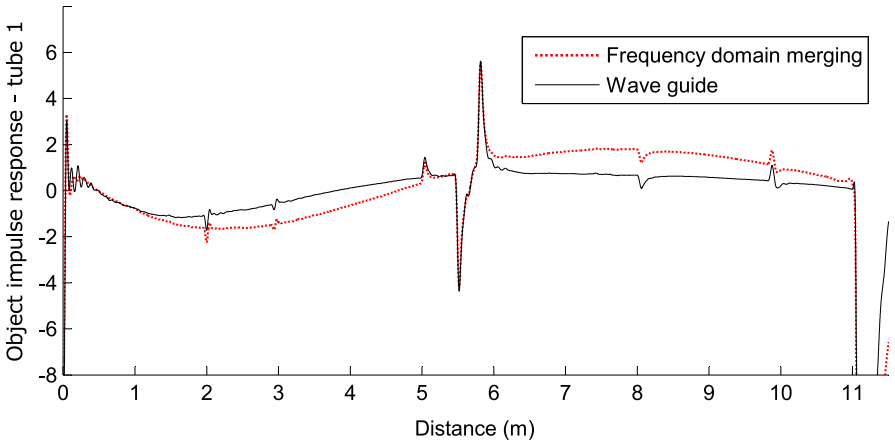

Figure 7: A comparison of the impulse responses of tube 1 when wave separation is performed using the two alternate algorithms

waveguide are hard to balance against the increased calibration and processing requirements.

5.3. Validation against theory

To validate the results obtained in Section 5.2 the acoustic impulse response of tube 1 was calculated using an acoustic tube simulator and compared to results obtained by experiment. The simulator was constructed according to [18, 21–23] where details of the algorithms may be found, a brief overview follows. The tube is discretised into cylindrical segments separated by nodes. Each segment was characterised by a digital FIR filter which characterises attenuation due to both viscous and thermal effects at the wall. Wall roughness effects [24] were not included in the simulation as the extruded tube has a smooth internal surface. The simulator accounts for changes in internal diameter by transforming the associated acoustic impedance changes into reflection and transmission coefficients that are applied at each node. To obtain the impulse response of tube 1, when connected to the source-tube as per the experimental measurement, a forward traveling pressure pulse of unity amplitude is applied at the node associated with microphone three and the resulting reflection sequence is recorded at the same location. To ensure that the test object impulse response is free of source re-reflections it is assumed that any sound that is reflected backwards and reaches the beginning of the source-tube is not then re-reflected back into the tube; this is easily implemented in simulation by setting the inward facing reflection coefficient at the first node to 0. Once the simulated impulse response of tube 1 was obtained, it was filtered using the same 100 order low pass FIR Chebyshev window filter that was used to filter the experimental data.

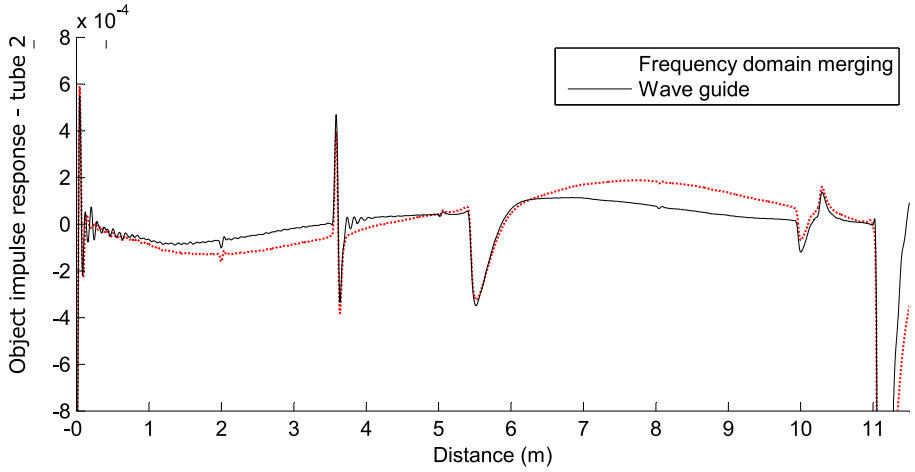

Figure 8: A comparison of the impulse responses of tube 2 when wave separation is performed using the two alternate algorithms

Figure 9 compares the simulated impulse response of tube 1 with the experimentally derived response, obtained using the waveguide method. Unfortunately it is difficult to gauge the accuracy of the experimental readings from the plot in Figure 9 due to the low frequency interference in the experimentally derived results. To remedy this problem a 7th order polynomial was fitted, using least squares, to the experimentally derived signal over the range 0.13 m to 10.75 m. The resulting polynomial curve was subtracted from the experimental signal giving a corrected experimental response that contains very little low frequency interference (Figure 10).

In Figure 10 it is clear to see that the corrected experimental readings replicates the simulated results well. Because the simulator is one dimensional in nature and therefore can only account for changes in internal diameter, the internal pit at 2394 mm was represented in simulation by matching the volumetric wall loss to an increase in internal diameter over a single segment length. The first zoomed section in Figure 10 show that the size, shape and location of the pit signal feature generated by the simulator is deftly replicated in the experimentally obtained signal. In the second zoomed section of Figure 10 it is shown that there is also a good match between simulation and experiment for the signal feature associated with the partial blockage at 9828 mm. Concerning the erosion at 5477 mm, it is clear that, although in general the experimental and simulated signal features correlate well, the experimentally derived signal has slightly higher peaks than those of the simulated response. This is most likely caused by tolerances of the internal diameter of the tube sections. The dimensions of the features machined into the tube are based upon the nominal diameter of the tube (18.8mm), therefore any variation in the internal diameter of the tube will cause inaccuracies in the sizing of features.

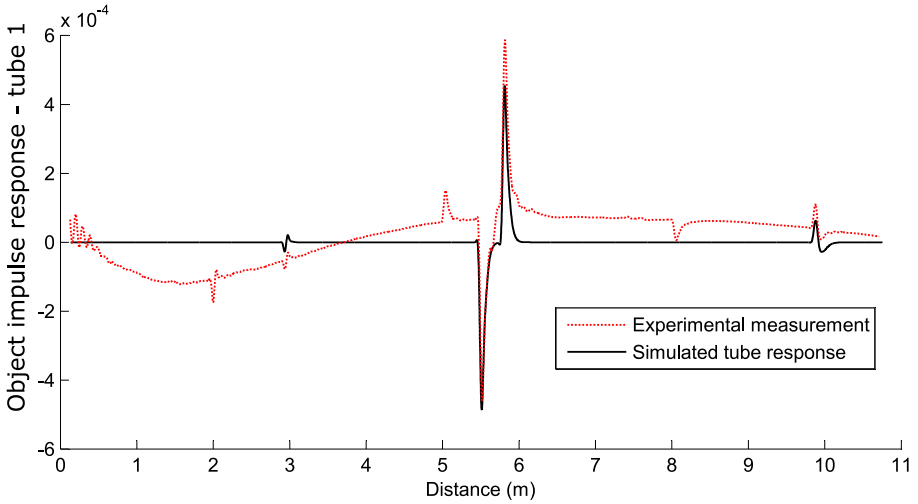

Figure 9: Comparison between experimentally derived and simulated acoustic impulse response signals of tube 1 - the usefulness of the plot is reduced by the presence of low frequency interference in the experimentally obtained signal

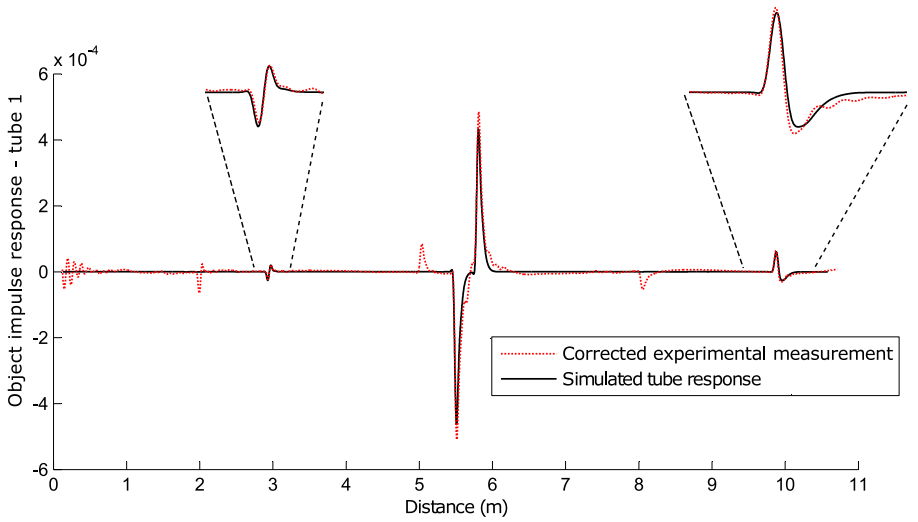

Figure 10: Comparison between the corrected experimentally obtained acoustic impulse response of tube 1 and the simulated response; low frequency interference has been removed from the experimental data by fitting a 7th order polynomial and removing the resulting curve from the signal

It is apparent from the signal features at the tube joins that the different tube sections do not have equal diameters; the features suggest that at the intersection at 2 m there is an increase in the internal diameter of tube 1, at 5 m there is a decrease and at 8 m the diameter increases again. Small variations in tube cross section at joint locations are expected due to the modular nature of the test rig and tolerances of the extruded tube.

6. Conclusions

The key facet of both of the wave separation methods developed, that stands apart from previous work [2, 4, 9–12], is that the techniques were designed such that they may be easily used in an industrial setting, where portability, speed and ease of use are important issues. The first method is an improved implementation of the work presented by Kemp et al. [2], while the second method is a development of the method of [4]. The improvements made to the work of Kemp et al. [2] allow simplified calibration and a more accurate means of determining the inter-microphone transfer functions. The development to the work of [4] offers practical benefits over the waveguide algorithm of Kemp et al. [2]: the technique sacrifices the inclusion of inter-microphone attenuation in favor of drastically simplified calibration; it also offers the benefit of algorithmic simplicity and as such reduced computational requirements.

It was demonstrated that all of the fabricated defects could be clearly identified, located and characterised using either separation algorithm. In experimental results from both separation algorithms a degree of low frequency interference was evident but the waveguide algorithm consistently showed lower levels of interference. The signals obtained by experiment were validated against results from a theoretically derived tubular acoustic simulator and it was shown that simulated acoustic impulse response signals matched very well with experimentally obtained data, provided low frequency drift in the experimental data was removed.

Neither of the wave separation techniques developed showed universal benefit over the other. The waveguide technique was less affected by low frequency interference and this was attributed to the inclusion of inter-microphone transfer functions. However, due to the use of inter-microphone transfer functions, the waveguide method requires on site calibration which is unfavorable in a industrial setting. The waveguide technique is better suited to the testing of individual tubes in a laboratory setting where time and equipment is available for detailed calibration, and computational cost of the separation algorithm is of little importance. It is also noted that the waveguide technique may give better results if the microphone spacing is increased or a smaller diameter source-tube is used, due to the subsequent increase in the effects of inter-microphone attenuation. The low computational cost of the frequency merging technique combined with its minimal calibration requirements makes it highly suited to industrial use. Computational savings, that make little odds in a laboratory,

can be of significant benefit if multiple tubes are tested at once or if the system is to be deployed on a low power processor such as those present on modern microcontrollers.

Acknowledgment

The authors would like to thank BP Exploration for funding the research and Phoenix Inspection Systems Limited for the use of their testing facilities.

[1] J. Buick, J. Kemp, D. Sharp, M. van Walstijn, D. Campbell, R. Smith, Distinguishing between similar tubular objects using pulse reflectometry: a study of trumpet and cornet leadpipes, Measurement Science and Technology 13 (5) (2002) 750.

[2] J. Kemp, M. van Walstijn, D. Campbell, J. Chick, R. Smith, Time domain wave separation using multiple microphones, The Journal of the Acoustical Society of America 128 (2010) 195.

[3] J.-P. Dalmont, M. Curtit, A. F. Yahaya, On the accuracy of bore reconstruction from input impedance measurements: Application to bassoon crook measurements, The Journal of the Acoustical Society of America 131 (1) (2012) 708–714.

[4] B. Louis, G. Glass, B. Kresen, J. Fredberg, Airway area by acoustic reflection: the two-microphone method, Journal of biomechanical engineering 115 (1993) 278.

[5] D. T. W. Chu, K. Li, J. Epps, J. Smith, J. Wolfe, Experimental evaluation of inverse filtering using physical systems with known glottal flow and tract characteristics, The Journal of the Acoustical Society of America 133 (5) (2013) EL358–EL362.

[6] X. Wang, K. M. Lewis, K. A. Papadopoulou, B. Lennox, J. T. Turner, Detection of hydrate and other blockages in gas pipelines using acoustic reflectometry, Proceedings of the Institution of Mechanical Engineers, Part C: Journal of Mechanical Engineering Science 226 (7) (2012) 1800–1810.

[7] K. Papadopoulou, M. Shamout, B. Lennox, D. Mackay, A. Taylor, J. Turner, X. Wang, An evaluation of acoustic reflectometry for leakage and blockage detection, Proceedings of the Institution of Mechanical Engineers, Part C: Journal of Mechanical Engineering Science 222 (6) (2008) 959–966.

[8] W. Duan, R. Kirby, J. Prisutova, K. V. Horoshenkov, On the use of power reflection ratio and phase change to determine the geometry of a blockage in a pipe, Applied Acoustics 87 (2015) 190 – 197.

[9] A. Li, D. B. Sharp, The problem of offset in measurements made using acoustic pulse reflectometry, Acta acustica united with acustica 91 (4) (2005) 789–796.

[10] M. van Walstijn, M. Campbell, J. Kemp, D. Sharp, Wideband measurement of the acoustic impedance of tubular objects, Acta acustica united with acustica 91 (3) (2005) 590–604.

[11] D. Sharp, D. Campbell, Leak detection in pipes using acoustic pulse reflectometry, Acta Acustica united with Acustica 83 (3) (1997) 560–566.

[12] P. Dickens, J. Smith, J. Wolfe, Improved precision in measurements of acoustic impedance spectra using resonance-free calibration loads and controlled error distribution, The Journal of the Acoustical Society of America 121 (3) (2007) 1471–1481.

[13] K. Groves, B. Lennox, Echo removal in tubular acoustic systems: Passive and active techniques, The Journal of the Acoustical Society of America 134(5) (2013) 4191.

[14] M. van Walstijn, G. de Sanctis, Adaptive calibration of a three-microphone system for acoustic waveguide characterization under time-varying conditions, The Journal of the Acoustical Society of America 135 (2) (2014) 917–927.

[15] S.-H. Jang, J.-G. Ih, On the multiple microphone method for measuring in-duct acoustic properties in the presence of mean flow, The journal of the acoustical society of America 103 (3) (1998) 1520–1526.

[16] J.-P. Dalmont, Acoustic impedance measurement, part i: A review, Journal of Sound and Vibration 243 (3) (2001) 427–439.

[17] J. A. Kemp, S. Bilbao, J. McMaster, R. A. Smith, Wave separation in the trumpet under playing conditions and comparison with time domain finite difference simulation, The Journal of the Acoustical Society of America 134 (2) (2013) 1395–1406.

[18] N. Amir, U. Shimony, G. Rosenhouse, Losses in tubular acoustic systems theory and experiment in the sampled time and frequency domains, Acta Acustica united with Acustica 82 (1) (1996) 1–8.

[19] D. H. Keefe, Acoustical wave propagation in cylindrical ducts: Transmission line parameter approximations for isothermal and nonisothermal boundary conditions, The Journal of the Acoustical Society of America 75 (1984) 58.

[20] N. Amir, D. Bobrow, T. Pechter, Applying acoustic pulse reflectometry in a geothermal energy plant: a case study, in: ASME 2010 Power Conference, American Society of Mechanical Engineers, 2010, pp. 431–434.

[21] D. Sharp, Acoustic pulse reflectometry for the measurement of musical wind instruments, Ph.D. thesis, The University of Edinburgh (1996).

[22] J. Kemp, Theoretical and experimental study of wave propagation in brass musical instruments, Ph.D. thesis, The University of Edinburgh (2002).

[23] N. Amir, U. Shimony, G. Rosenhouse, A discrete model for tubular acoustic systems with varying cross section the direct and inverse problems. part 1: Theory, Acta Acustica united with Acustica 81 (5) (1995) 450–462.

[24] A. Krynkin, K. V. Horoshenkov, S. J. Tait, An eigenvalue correction due to scattering by a rough wall of an acoustic waveguide, The Journal of the Acoustical Society of America 134 (2) (2013) 939–949.

AppendixA. Wave separation technique of Louis et al.

Louis et al. [4] use a two microphone technique to determine the impulse response of tubular objects. The application is imaging of human airway geometry; as such a miniaturised apparatus is constructed using a headphone type loudspeaker attached to a 12 mm source-tube that houses two transducers. The technique relies on the assumption that there are no losses between the two microphones and that the pressure field in the source-tube can be described by the superposition of two one-dimensional waves propagating at the same speed but in opposite directions:

$$p_x(t) = p_x^+(t) + p_x^-(t) \tag{A.1}$$

where $p_x^+(t)$ is the wave propagating to the right at axial location x, $p_x^-(t)$ is the wave propagating to the left at axial location x and $p_x(t)$ is the pressure at location x. Defining τ as the propagation delay between the two microphones it is possible to define:

$$p_{x_2}^+(t) = p_{x_1}^+(t-\tau) \tag{A.2}$$

$$p_{x_2}^-(t) = p_{x_1}^-(t+\tau) \tag{A.3}$$

where subscripts x_1 and x_2 refer to the microphone locations. $p_x^+(t)$ and $p_x^-(t)$ are related by the impulse responses of the system on either side of the microphones:

$$p_{x_2}^-(t) = p_{x_2}^+(t) \star h(t) \tag{A.4}$$

$$p_{x_2}^+(t) = p_{x_2}^-(t) \star s(t) \tag{A.5}$$

where $h(t)$ is the impulse response of the part of the system lying in the domain $x \geq x_2$, $s(t)$ is the impulse response of the part of the system in the domain $x \leq x_2$ and $\star$ represents convolution. Rearranging Equations (A.1), (A.2) and (A.3)

to express pressures at the measurement sites in terms of the forward and backward travelling waves at location x_2:

$$p_{x_1}(t) = p^+_{x_2}(t+\tau) + p^-_{x_2}(t-\tau) \tag{A.6}$$

$$p_{x_2}(t-\tau) = p^+_{x_2}(t-\tau) + p^-_{x_2}(t-\tau) \tag{A.7}$$

$$p_{x_2}(t+\tau) = p^+_{x_2}(t+\tau) + p^-_{x_2}(t+\tau) \tag{A.8}$$

Subtracting Equation (A.7) from Equation (A.6) and Equation (A.6) from Equation (A.8):

$$p_{x_1}(t) - p_{x_2}(t-\tau) = p^+_{x_2}(t+\tau) - p^+_{x_2}(t-\tau) \tag{A.9}$$

$$p_{x_2}(t+\tau) - p_{x_1}(t) = p^-_{x_2}(t+\tau) - p^-_{x_2}(t-\tau) \tag{A.10}$$

Finally, from Equations (A.9), (A.10) and (A.4):

$$h(t) \star \left[p^+_{x_2}(t+\tau) - p^+_{x_2}(t-\tau)\right] = \left[p^-_{x_2}(t+\tau) - p^-_{x_2}(t-\tau)\right] \tag{A.11}$$

which is simply an expansion of Equation (A.4). Rearranging Equation (A.11) using Equations (A.9) and (A.10):

$$h(t) \star \left[p_{x_1}(t) - p_{x_2}(t-\tau)\right] = \left[p_{x_2}(t+\tau) - p_{x_1}(t)\right] \tag{A.12}$$

Equation (A.12) is in terms of measured microphone signals and a known time delay. It may be solved for the impulse response $h(t)$ using an appropriate deconvolution algorithm.